

Sustainable Synthesis and Structural Characterization of Carbon, Graphite, Graphene Oxide, and Reduced Graphene Oxide Derived from Coconut Shells

Husain Husain^{1*}, Irwan Ramli², Wisnu Ari Adi³, Yunasfi Yunasfi³, Mashadi Mashadi³, Ade Mulyawan³, Didin Sahidin Winatapura³, Subaer Subaer¹, Yana Taryana⁴, Yuyu Wahyu⁴, Nurmala Dewi¹, and Agus Susanto¹

¹Department of Physics, Faculty of Mathematics and Natural Sciences, Universitas Negeri Makassar, Jl. A.P. Pettarani, Makassar 90222, Indonesia

²Department of Physics, Faculty of Science, Universitas Cokroaminoto Palopo, Jl. Latamacelling, Palopo 91921, Indonesia

³Center for Research and Technology of Nuclear Advanced Materials, National Research and Innovation Agency, Jl. Raya Puspitek, Tangerang Selatan, Banten 15310, Indonesia

⁴Research Center for Electronics and Telecommunication, National Research and Innovation Agency, Jl. Sangkuriang, Bandung 40135, Indonesia

* Corresponding author:

tel: +62-81342712344

email: husain.physics@unm.ac.id

Received: March 17, 2025

Accepted: August 28, 2025

DOI: 10.22146/ijc.105467

Abstract: This study explores the sustainable synthesis and structural characterization of carbon, graphite, graphene oxide (GO), and reduced graphene oxide (rGO) derived from coconut shells. The objective is to investigate the potential of biomass-based precursors to produce functional carbon materials through controlled chemical treatments. X-ray diffraction patterns of carbon and graphite exhibit broad peaks, indicating low crystallinity and amorphous characteristics, while GO and rGO show dominant peaks at 22° and 23°, corresponding to the (002) plane. Scanning electron microscopy confirms the disordered morphology of carbon and graphite, while high-resolution transmission electron microscopy reveals wrinkled GO sheets and partially restacked rGO layers. Fourier transform infrared spectra identify O–H stretching at $\sim 3442\text{ cm}^{-1}$ in carbon and C=C stretching at 1630 cm^{-1} in graphite, along with various oxygen-containing functional groups in GO and rGO. Raman spectroscopy shows a sharp G band at 1580 cm^{-1} in graphite ($I_D/I_G = 0.840$), increased disorder in GO ($I_D/I_G = 0.843$), and partial graphitic restoration in rGO ($I_D/I_G = 0.841$). These findings confirm the successful transformation of coconut shells into valuable carbon-based materials and highlight their potential for use in sustainable energy and electronic applications.

Keywords: coconut shell; carbon; graphite; GO; rGO; structural characterization

■ INTRODUCTION

The quest for sustainable and environmentally friendly materials has increased interest in utilizing agricultural waste as a raw material for advanced technological applications. Among various agro-waste products, coconut shells have gathered significant attention due to their high carbon content and abundant availability [1-2]. Indonesia has a coconut plantation area of 3.6 million hectares, which annually produces 15.3 billion tons of coconuts. This amount of coconut shell

waste produced is around 3.6 million tons annually. With a carbon percentage reaching 50–60% from coconut shell waste [3], coconut shells are a very promising source of carbon. As an abundant agricultural by-product, coconut shells offer a sustainable and cost-effective source of carbon materials, reducing reliance on expensive and non-renewable commercial graphite precursors. The unique properties of carbon derived from coconut shells, such as their inherent structural disorder and tunable characteristics [4], make them

suitable for advanced material applications. The ecological benefits of utilizing biomass waste for high-value material synthesis align with global sustainability goals.

Carbon materials like graphite, graphene oxide (GO), and reduced graphene oxide (rGO) have exceptional electrical [5], thermal and mechanical properties [6], making them ideal for various applications, including electronics [7], energy storage [8], and sensors [9]. GO is an oxidized form of graphene that contains various oxygen-containing functional groups, such as hydroxyl, epoxy, and carboxyl [10]. These functional groups make GO highly dispersible in water and other solvents, facilitating its processing and application [11]. Meanwhile, rGO is obtained by reducing the oxygen of GO, partially restoring the graphene structure and its conductive properties [12].

Although numerous studies have employed coconut shell as a carbon precursor, the novelty of this research lies in its systematic investigation of the structural transformation pathway from amorphous carbon to low-crystallinity graphite, GO, and rGO. Unlike previous works that often focus on end-use applications or single-stage synthesis, this study uniquely tracks and analyzes each intermediate phase using comprehensive structural characterizations such as X-ray diffraction (XRD), Fourier transform infrared (FTIR), scanning electron microscopy (SEM), high-resolution transmission electron microscopy (HRTEM), and Raman spectroscopy. Furthermore, this work highlights how the low crystallinity of biomass-derived graphite affects the oxidation and reduction behavior of GO and rGO, leading to distinct structural and chemical features not typically reported in studies using commercial graphite. By combining sustainable synthesis with in-depth structural analysis, this research provides new insight into the fundamental material evolution and offers a scalable route for producing tunable carbon-based nanomaterials from biomass.

■ EXPERIMENTAL SECTION

Materials

The materials used in this research included HF (40%), H₃PO₄, H₂SO₄, KMnO₄, and H₂O₂, all pro-analysis grade with high purity.

Instrumentation

Many measurements were conducted to investigate the structural evolution of carbon, graphite, GO, and rGO. The crystal structure evolution from carbon, graphite, GO, and rGO was investigated using XRD. XRD measurements were performed using a Model X'Pert MPD X-ray diffractometer. The diffractometer had a Cu K α radiation source ($\lambda = 1.5406$ Å). Diffraction patterns were recorded over a 2θ range of 10° to 55° , with a step size of 0.02° and a counting time of 1 second per step. The X-ray tube was operated at 40 kV and 30 mA.

Meanwhile, the functional groups of each sample were studied using FTIR. FTIR spectroscopy measurements were carried out using a Model ThermoScientific Nicolet iS10 FTIR spectrometer. The system was purged with dry air to remove CO₂ and H₂O interferences. Spectra were recorded in the mid-infrared region (4000 – 1000 cm⁻¹) with a resolution of 4 cm⁻¹. A background spectrum was collected before each sample measurement using a clean KBr pellet to account for atmospheric contributions. The spectra were automatically ratioed against the background to yield absorbance spectra.

SEM analysis was performed using a Hitachi SU-3500 model. The electron beam was operated at an accelerating voltage of 15 kV and a working distance of 10 mm. HRTEM analysis was performed using a Tecnai G² 20 S-TWIN Transmission Electron Microscope. The instrument was equipped with a LaB₆ electron source and a high-resolution CCD camera for image capture. The electron beam was operated at an accelerating voltage of 200 kV. The focus and alignment of the electron beam were meticulously adjusted to achieve optimal image resolution. Lastly, Raman spectroscopy measurements were conducted using a Horiba Type MFO Raman spectrometer. The laser beam was focused onto the sample using a 50 \times objective lens. The laser power at the sample was maintained at 10 mW to prevent sample degradation. Spectra were collected over a wavenumber range of 500 to 2500 cm⁻¹ to cover the relevant vibrational modes of the samples.

Procedure

Synthesis of carbon

The synthesis of carbon began with the preparation of coconut shells as the raw material. The shells were mechanically cleaned to remove any organic residues or contaminants. Afterwards, they were crushed and ground into smaller particles to increase the surface area and ensure uniform carbonization. The ground coconut shells were then subjected to a carbonization process at 600 °C for 3 h. The high-temperature treatment decomposed the organic matter, leaving behind carbon-rich material. Once carbonization was complete, the material was cooled to room temperature without oxygen to prevent oxidation. The resulting carbon powder was collected and stored for subsequent processing.

Synthesis of graphite

The carbon powder obtained from the first stage was sieved through a 200-mesh sieve to ensure particle uniformity. Approximately 30 g of the sieved carbon powder was stirred in a 40% HF solution (100 mL) at 45 °C for 3 h at 600 rpm—the acid treatment aimed to remove any remaining impurities and improve the purity of the carbon material. The treated sample was washed multiple times with distilled water until it reached a neutral pH to ensure no residual acids remained. After washing, the sample was dried at 110 °C for 12 h to remove residual moisture. Finally, the dried carbon powder was calcined at 750 °C for 5 h to facilitate the transformation into graphite powder.

Synthesis of GO

The synthesis of GO was carried out using a modified Hummers method. Initially, 3 mL of H₃PO₄ and 27 mL of H₂SO₄ were mixed and stirred at 300 rpm for 10 min in an ice bath to maintain a low reaction temperature. Subsequently, 1 g of KMnO₄ was gradually added to the acid mixture, followed by the slow addition of 3 g of graphite powder while maintaining the temperature below 20 °C to prevent uncontrolled exothermic reactions. The mixture was stirred continuously for 3 h to ensure proper oxidation of the graphite layers. After oxidation, the reaction was quenched by slowly adding 200 mL of deionized water and 3 mL of H₂O₂ (30% w/w), which resulted in a

noticeable color change to bright yellow, indicating the formation of GO. The suspension was washed multiple times with deionized water through centrifugation at 4000 rpm for 10 min until the supernatant reached a neutral pH. Finally, the residue was dried at 60 °C for 24 h to yield GO powder.

Synthesis of rGO

The synthesis of rGO involved the chemical reduction of GO. First, 0.5 g of GO powder was dispersed in 100 mL of deionized water using ultrasonication for 30 min to ensure uniform dispersion of the GO sheets. The dispersion was then transferred into an acrylic autoclave reactor and heated at 160 °C for 6 h to facilitate the reduction process. After the heating process, the reactor was cooled to room temperature, and the resulting material was filtered and washed with deionized water to remove any residual by-products or unreacted chemicals. Finally, the product was dried at 60 °C for 12 h in a vacuum oven to produce rGO powder.

RESULTS AND DISCUSSION

Crystal Structure Analysis

XRD analysis was performed to investigate the crystal structure of all materials. The XRD patterns of carbon, graphite, GO, and rGO are presented in Fig. 1. The XRD pattern of carbon exhibits broad peaks (Fig. 1(a)), revealing an amorphous structure. The lack of diffraction peaks indicates that carbon is primarily non-crystalline. This is an expected result for carbonized biomass materials since the structure has no long-range order [13]. The XRD pattern of graphite powders (Fig. 1(b)) shows two dominant mounds without sharp peaks, indicating a low degree of crystallization [14]. These results differ from several sources, which state that graphite has a crystalline phase [15-16]. This occurs because the graphite in this study was obtained from natural materials with a low crystallinity level. The sample's amorphous nature prevents it from having well-ordered crystalline structures, which inhibits it from having identifiable diffraction peaks. Wachid et al. [13] reported similar results with the same XRD pattern. This approach demonstrates an eco-friendly and cost-effective route for producing advanced carbon materials,

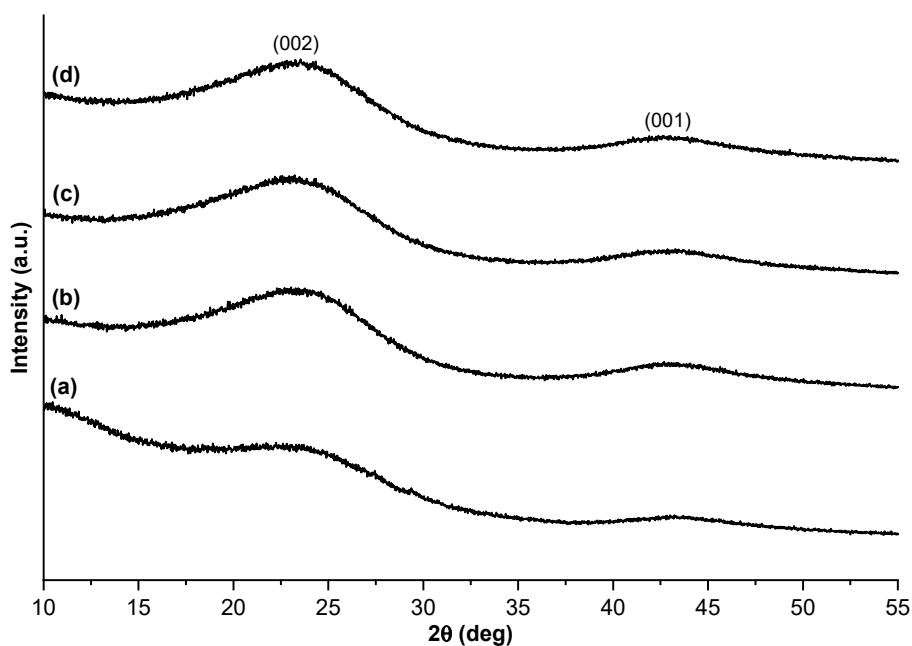


Fig 1. The XRD pattern of (a) carbon, (b) graphite, (c) GO, and (d) rGO

contributing to the development of sustainable material science while offering tailored structural properties for specific applications.

The XRD pattern of GO observed in this study shows a distinct peak at around 22° (Fig. 1(c)), which differs from many studies where GO typically exhibits a prominent peak at approximately 11° due to the (002) plane [17-18]. In this research, the peak at 22° suggests a reduced interlayer distance, which is more similar to patterns observed in graphite studies with a lower degree of crystallinity [19]. This difference is attributed to the starting material used in the synthesis process; graphite with high crystallinity leads to a well-defined GO structure. In contrast, the coconut shell-derived graphite in this study has a lower crystallinity degree, as confirmed by XRD analysis, with an estimated crystalline content of around 34%. This results in GO with a broader peak around 22°, reflecting less structural order and lower oxidation levels compared to GO synthesized from highly crystalline graphite. This suggests that the initial structure and crystallinity of the precursor graphite play a significant role in determining the XRD profile of the resulting GO. Meanwhile, the XRD pattern of rGO (Fig. 1(d)) shows a broad peak centered around 23.3°, attributed to the (002) plane of rGO. The reduction process removes

some of the oxygen-containing groups, decreasing the interlayer spacing and restoring the conjugated network of carbon atoms. These XRD data demonstrate that graphite may structurally convert into GO and rGO even with a low-crystallinity precursor.

The XRD patterns of graphite, GO, and rGO derived from coconut shell biomass appear broad and partially overlapping due to the inherently low crystallinity of the precursor material. The transformation from graphite to GO and rGO is not marked by drastic shifts but by subtle and quantifiable changes in peak characteristics. The (002) peak of graphite is observed at 24.06°, with a full-width at half maximum (FWHM) of approximately 5.2° and a normalized intensity of 100%. After oxidation, GO exhibits a broad diffraction peak centered at 23.1°, with an increased FWHM of about 6.9° and a reduced intensity of approximately 64%, indicating interlayer expansion and structural disorder caused by the introduction of oxygen-containing functional groups. In rGO, the main peak reappears at 23.3°, with a FWHM of around 6.2° and relative intensity of about 70%, suggesting partial restoration of the graphitic structure through the removal of oxygen functionalities. These trends are consistent with previous reports, showing that

biomass-derived or low-crystallinity graphite precursors yield GO and rGO with broadened and less intense XRD peaks [20-21].

Functional Group Analysis

The FTIR spectra of carbon, graphite, GO, and rGO are shown in Fig. 2. The FTIR spectrum of carbon (Fig. 2(a)) reveals the O–H stretching vibrations at about 3442 cm^{-1} and stretching vibrations of C=C at 1567 cm^{-1} [22]. Meanwhile, the C–O stretching vibrations shown by the peaks at 1050 cm^{-1} are indications of some remaining oxygen-containing groups in the carbonized material [23]. The FTIR spectrum of graphite is shown in Fig. 2(b), and the spectrum is less prominent than that of the other samples, suggesting a lack of substantial functional groups. Weak bands at 3444 cm^{-1} (O–H stretching) and 1567 cm^{-1} (C=C stretching) indicate a graphitic structure that is primarily unfunctionalized and has few oxygen-containing groups [24].

The FTIR spectrum of GO exhibits several distinctive peaks corresponding to various oxygen-containing functional groups (Fig. 2(c)). The broad peak at approximately 3463 cm^{-1} is attributed to O–H stretching vibrations [22]. The 1720 and 1624 cm^{-1} peaks correspond to C=O stretching vibrations from carboxyl and carbonyl groups [25]. The peak at 1220 cm^{-1} is associated with C–O–H stretching, while the peak at 1050 cm^{-1} is attributed to C–O stretching vibrations [26]. The carbon and graphite spectra appear similar due to overlapping peaks. However, the C=C stretching vibration around 1630 cm^{-1} in carbon appears broader and less intense. Meanwhile, the same C=C peak in graphite is sharper and more intense, indicating a higher degree of graphitization and more ordered carbon domains. These peaks confirm the successful oxidation of graphite to GO, presenting multiple oxygen functionalities in the structure.

The FTIR spectrum of rGO (Fig. 2(d)) shows a significant reduction in the intensity of oxygen-containing functional groups, particularly at 3462 , 1713 , 1223 , and 1117 cm^{-1} , compared to GO. The FTIR spectrum of rGO demonstrates a notable reduction in O–H stretching vibrations near 3462 cm^{-1} , consistent with the removal of hydroxyl groups during the reduction process, as previously reported [20-21]. The C=O stretching peak

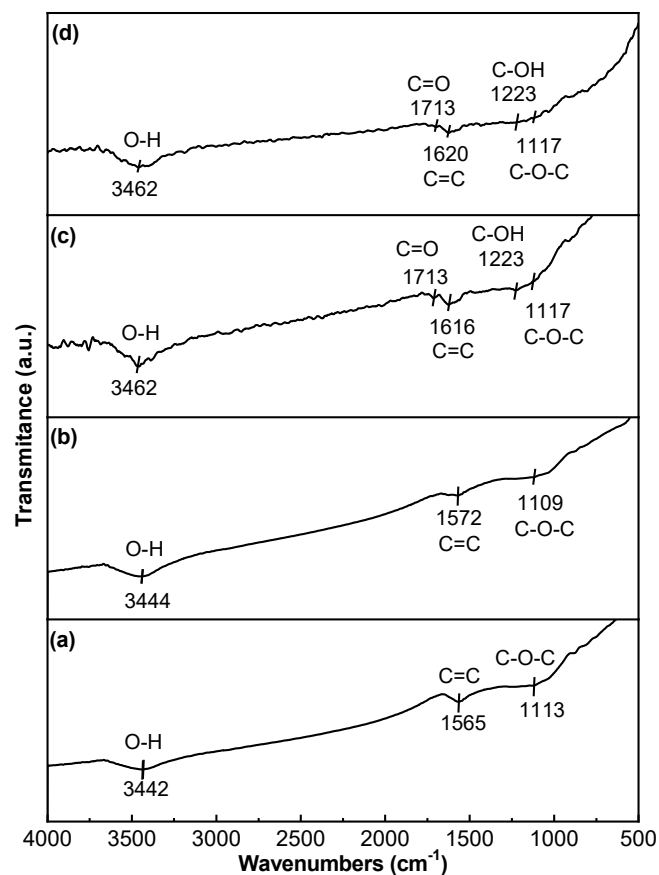


Fig 2. FTIR spectrum of (a) carbon, (b) graphite, (c) GO, and (d) rGO

at 1713 cm^{-1} , prominent in GO, is significantly diminished in rGO, indicating the effective removal of carboxyl groups. In addition, the C–O–H and C–O–C stretching vibrations at 1223 and 1117 cm^{-1} , respectively, show decreased intensities, suggesting a partial restoration of the sp^2 carbon network. These changes collectively confirm the successful reduction of GO to rGO. The observed spectral evolution is consistent with previous studies and aligns with the XRD results, which also reflect structural changes and partial graphitization during reduction [27-28].

Micro and Nanostructure Analysis

Fig. 3 shows the micro and nanostructure of carbon, graphite, GO, and rGO. SEM images of carbon and graphite (Fig. 3(a) and 3(c)) exhibit a mostly amorphous structure. In this study, the SEM images of carbon and graphite exhibit irregular, disordered surface textures consistent with the low-crystallinity and

amorphous characteristics confirmed by XRD analysis. Thus, the SEM observations complement the diffraction data by visually reinforcing the structural disorder present in these materials. This lack of crystallinity is consistent with the broad peaks observed in the XRD analysis. The amorphous nature of the carbon suggests a disordered arrangement of carbon atoms, which is typical for carbonized biomass materials [29]. The SEM analysis reveals the amorphous nature of carbon and the relatively disordered structure of graphite, as evidenced by the irregular and rough surface features. The corresponding EDX spectrum of carbon (Fig. 3(b)) confirms the dominant presence of carbon as the primary element, with negligible signals from other components, indicating high purity of the synthesized carbon. This result supports the effectiveness of the carbonization process in removing most heteroatoms, consistent with the structural characterization results.

The HRTEM images of GO (Fig. 3(d)) reveal thin and wrinkled sheets with a large surface area, characteristic of exfoliated graphene oxide layers [30]. The individual

GO sheets are observed to be separated, confirming the successful oxidation and exfoliation process. The HRTEM images of rGO (Fig. 3(e)) show partially restacked layers that are less wrinkly and flawed than GO. The reduction process partially restores the graphitic structure, as the graphene layers in rGO appear better ordered and less wrinkled compared to GO. However, some residual defects and disordered regions remain, indicating that the reduction is incomplete. The thinner and more transparent sheets of rGO, as seen in the HRTEM image, suggest improved layer separation compared to the thicker, more wrinkled morphology of GO. This observation is consistent with previous reports, such as Zhang et al. [20], who observed similar wrinkled and exfoliated GO layers due to oxidation-induced structural disruption, and Stankovich et al. [21], who reported that rGO exhibits smoother and more compact features after chemical reduction. The microstructural evolution from carbon to graphite, GO, and rGO, as shown in the SEM and HRTEM images, demonstrates the significant impact of chemical treatments on morphology

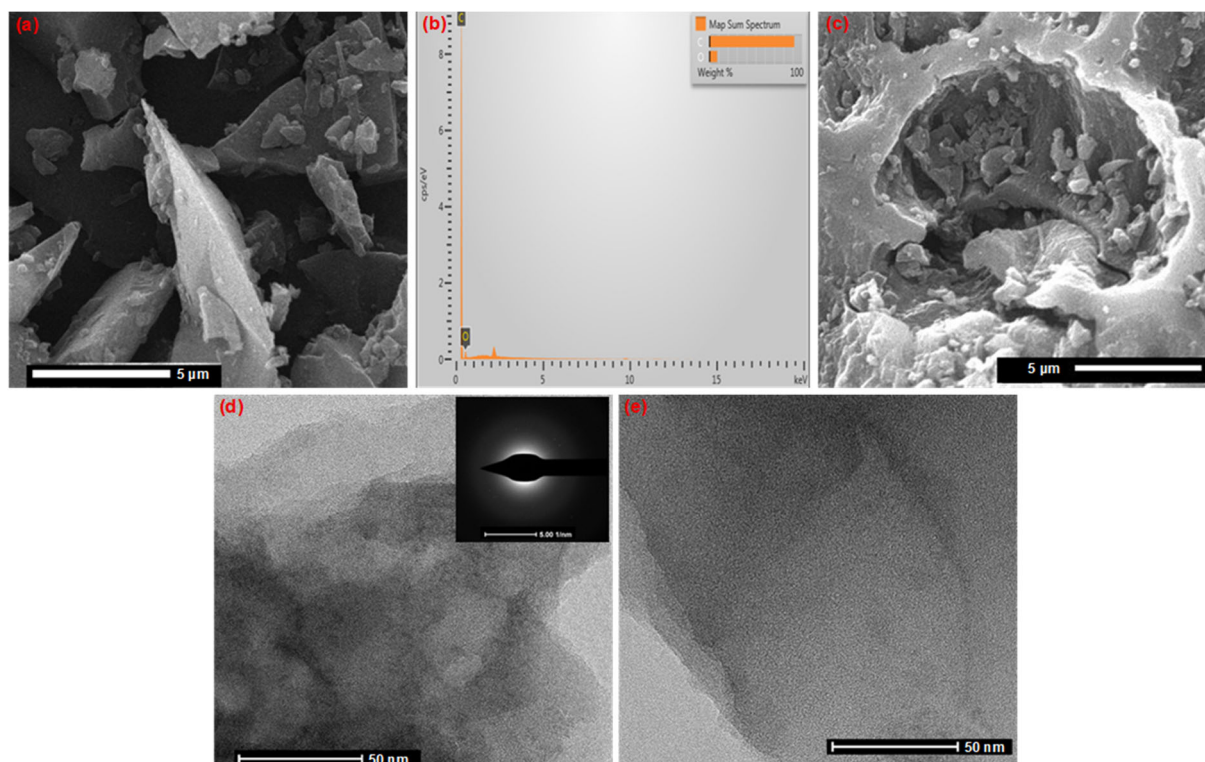


Fig 3. SEM images of (a) carbon (magnification: 5000 \times) with (b) the EDX results and (c) graphite (magnification: 5000 \times), as well as HRTEM images of (d) GO, and (e) rGO

and structural ordering. The fragmented and amorphous structure of carbon transitions into a more layered arrangement in graphite, reflecting partial crystallinity. Oxidation during GO synthesis introduces functional groups and defects, while the subsequent reduction step partially restores the graphitic lattice, leading to more compact stacking and reduced defect density.

Raman Spectroscopy Analysis

The Raman spectra of graphite, GO, and rGO are presented in Fig. 4. The Raman spectrum of graphite, with a sharp and intense G band around 1580 cm^{-1} , indicates a high degree of graphitization and fewer structural defects [31]. The lower intensity of the D band relative to the G band (I_D/I_G ratio) specifies minimal disorder in the material [32-33]. In contrast, the Raman spectrum of GO shows prominent D and G bands, but the I_D/I_G ratio is higher than that of graphite. This increased ratio points to a greater density of defects and disorder, primarily due to introducing oxygen-containing functional groups during oxidation. These functional groups disrupt the sp^2 carbon network, leading to more defects in the GO structure [34].

A partial reduction of defects is indicated by the Raman spectra of rGO, which shows both D and G bands and a lower I_D/I_G ratio than GO. Based on these data, some

of the oxygen-containing functional groups that cause the sp^2 carbon network to break have been successfully eliminated throughout the reduction process, improving structural order. The I_D/I_G ratio reduction shows that the disorder has decreased, indicating the restored graphitic structure. The fact that the I_D/I_G ratio of rGO is still more significant than the I_D/I_G ratio of graphite suggests that the material still has some residual flaws [35].

In this study, graphite exhibits an I_D/I_G ratio of 0.840, indicating a lower defect density and relatively ordered graphitic structure. For GO, the I_D/I_G ratio increases slightly to 0.843, reflecting the higher defect density caused by oxygen-containing functional groups introduced during the oxidation process. After the reduction process, rGO shows an I_D/I_G ratio of 0.841, suggesting partial restoration of the graphitic structure while retaining some structural defects.

The Raman analysis reveals that the I_D/I_G values of graphite, GO, and rGO exhibit minimal variation, which can be attributed to the low crystallinity of the precursor graphite derived from coconut shells. Unlike highly crystalline graphite, where oxidation and reduction processes significantly alter the defect density, low-crystallinity graphite already possesses many structural

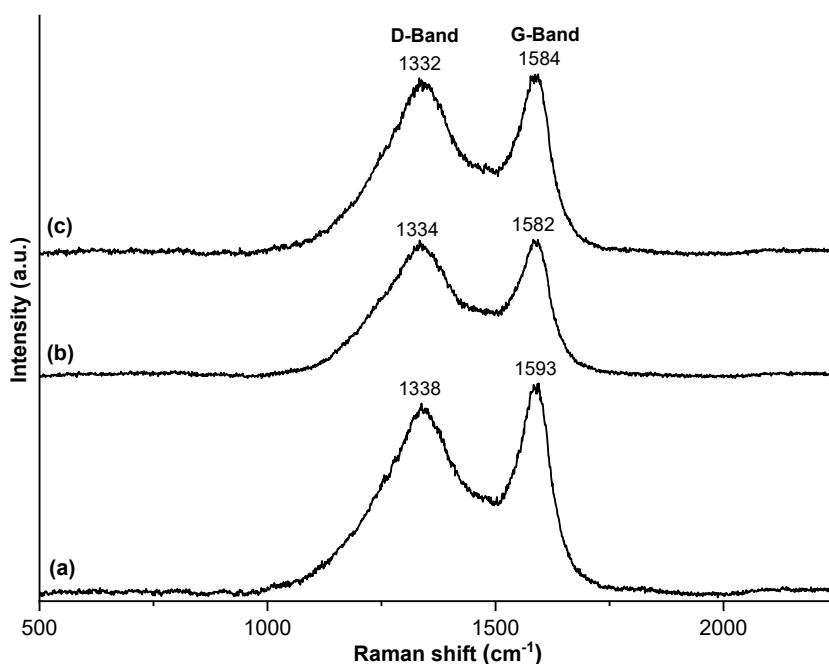


Fig 4. Raman spectroscopy of (a) graphite, (b) GO, and (c) rGO

defects. As a result, the introduction of oxygen-containing functional groups during the oxidation of graphite to GO and the subsequent partial reduction to rGO does not create significant changes in the overall defect density, thus resulting in similar I_D/I_G values across these materials.

The yield at each stage of the synthesis process was determined by comparing the mass of the final product to the initial material after complete washing and drying. The synthesis of graphite from coconut shell-derived carbon resulted in a yield of approximately 85%. In comparison, the subsequent conversion to GO yielded around 70%, and the final reduction to rGO achieved a yield of 60%. These values reflect the effectiveness of each chemical treatment step in retaining material mass while introducing or removing functional groups. The relatively high yields throughout the process suggest that coconut shell-derived carbon is a viable and efficient precursor for producing graphene-based materials, supporting its potential for scalable and sustainable applications.

■ CONCLUSION

Using a biomass precursor that is both affordable and sustainable, this study effectively synthesized and thoroughly characterized carbon, graphite, GO, and rGO obtained from coconut shells. The structural characteristics of the synthesized materials were strongly influenced by the degree of crystallinity of the precursor graphite, as observed through comparative analysis of XRD peak sharpness, FTIR functional group intensity, and microstructural differences in SEM and HRTEM images. The existence of oxygen-containing functional groups in GO was confirmed by FTIR spectroscopy. These groups were considerably less in rGO, indicating a partial restoration of the graphitic structure. SEM and HRTEM investigations revealed partially recovered graphene layers in rGO, an amorphous structure in carbon, well-ordered stacked layers in graphite, and exfoliated sheets with flaws in GO. The sample defect density and degree of graphitization were revealed by Raman spectroscopy, with the GO having a high I_D/I_G ratio. Alongside, rGO showed a reduced I_D/I_G ratio, indicating a partial restoration of structural order. These results show that materials generated from coconut shells

have the potential for advanced applications even in the presence of a lack of crystallinity in the precursor.

■ ACKNOWLEDGMENTS

This research was jointly funded by *Kementerian Pendidikan, Kebudayaan, Riset, dan Teknologi* of Indonesia through the Fundamental Research Grant (Contract No. 2879/UN36.11/LP2M/2024) and the National Research and Innovation Agency (BRIN) through the RIIIM III Grant (Contract No. 56/IV/KS/05/2023). We express our sincere gratitude for the invaluable support that has been instrumental in completing this project.

■ CONFLICT OF INTEREST

The authors have no conflict of interest.

■ AUTHOR CONTRIBUTIONS

Husain Husain conceptualized the research and manuscript writing. Irwan Ramli was responsible for characterization and analysis. Wisnu Ari Adi performed Raman spectroscopy, Yunasfi conducted the SEM, Mashadi conducted HRTEM, Ade Mulyawan data interpretation, Didin Sahidin Winatapura assisted in material synthesis, and Subaer contributed to optimization of experimental parameters. Yana Taryana and Yuyu Wahyu analyzed the electromagnetic properties, Nurmal Dewi and Agus Susanto reviewed and edited the manuscript, ensuring clarity and coherence. All authors read and agreed to the final version of this manuscript.

■ REFERENCES

- [1] Lejano, B., Elevado, K.J., Fandiño, M.A., Ng, E.A., Nicole Datinguino, Z.A., and Oliveros, S.B., 2024, Experimental investigation of utilizing coconut shell ash and coconut shell granules as aggregates in coconut coir reinforced concrete, *Cleaner Eng. Technol.*, 21, 100779.
- [2] Liang, X., Han, M., Xu, Z., Wang, R., and Yang, Z., 2024, Insight into the tribological performances of coconut shells as a potential natural water lubrication material, *Wear*, 546-547, 205350.

- [3] Priya, A.B., Shri, G.K.R., Dineshkumar, M., Romi, J.N., Nepolean, A.V., and Kirubakaran, V., 2020, Bio char and syngas production from coconut shell by pyrolysis: An experimental study, *AIP Conf. Proc.*, 2225, 040004.
- [4] He, P., Fu, G., Zhang, Y., Wang, Y., Yu, G., and Wu, G., 2024, Esterification of caprylic acid with glycerol for medium chain glycerides production catalyzed by waste coconut shell derived sulfonated carbon catalysts, *J. Environ. Chem. Eng.*, 12 (6), 114849.
- [5] Lalire, T., Longuet, C., and Taguet, A., 2024, Electrical properties of graphene/multiphase polymer nanocomposites: A review, *Carbon*, 225, 119055.
- [6] Wang, B., Li, N., Bao, Q., Cheng, S., Feng, J., Li, M., Wang, N., Wang, Z., Jiang, B., Chen, L., Hong, H., and Jian, X., 2024 Graphene at different scales to synergistically optimize the thermal and mechanical properties of CF/PPBESK composites, *Composites, Part B*, 284, 111692.
- [7] Yang, H., Zheng, H., Duan, Y., Xu, T., Xie, H., Du, H., and Si, C., 2023, Nanocellulose-graphene composites: Preparation and applications in flexible electronics, *Int. J. Biol. Macromol.*, 253, 126903.
- [8] Carrasco, D.F., Álvarez-Rubiera, E., Villar-Rodil, S., Martínez-Jódar, A., Tascón, J.M.D., Suárez-García, F., and Paredes, J.I., 2024, Chemically tuning graphene via anodic exfoliation for enhanced performance in aqueous zinc-based electrochemical energy storage applications, *Carbon*, 228, 119293.
- [9] Roy, S., 2024, Magnetic dipole and magnetic quadrupole scattering enhanced graphene-based tunable plasmonic metasurface- design and sensor applications, *Optik*, 311, 171947.
- [10] Khine, Y.Y., Wen, X., Jin, X., Foller, T., and Joshi, R., 2022, Functional groups in graphene oxide, *Phys. Chem. Chem. Phys.*, 24 (43), 26337–26355.
- [11] Ahmad, R.T.M., Hong, S.H., Shen, T.Z., and Song, J.K., 2016, Water-assisted stable dispersal of graphene oxide in non-dispersible solvents and skin formation on the GO dispersion, *Carbon*, 98, 188–194.
- [12] Oruç, S., Boztepe, C., and Zengin, R., 2023, Development electrically conductive PAAm/Alg/CNC/rGO/PANI hydrogel composites and investigation their bioelectronic properties, *Mater. Today Commun.*, 36, 106540.
- [13] Wachid, F.M., Perkasa, A.Y., Prasetya, F.A., Rosyidah, N., and Darminto, D., 2014, Synthesis and characterization of nanocrystalline graphite from coconut shell with heating process, *AIP Conf Proc.*, 1586 (1), 202–206.
- [14] Peng, W., Han, G., Huang, Y., Cao, Y., and Song, S., 2018, Insight the effect of crystallinity of natural graphite on the electrochemical performance of reduced graphene oxide, *Results Phys.*, 11, 131–137.
- [15] Nakayasu, Y., Goto, Y., Katsuyama, Y., Itoh, T., and Watanabe, M., 2022, Highly crystalline graphite-like carbon from wood via low-temperature catalytic graphitization, *Carbon Trends*, 8, 100190.
- [16] Kim, M.I., Cho, J.H., Hwang, J.U., Bai, B.C., and Im, J.S., 2021, Preparation of high-crystallinity synthetic graphite from hard carbon-based carbon black, *Appl. Phys. A: Mater. Sci. Process.*, 127 (2), 156.
- [17] Stobinski, L., Lesiak, B., Malolepszy, A., Mazurkiewicz, M., Mierzwa, B., Zemek, J., Jiricek, P., and Bieloshapka, I., 2014, Graphene oxide and reduced graphene oxide studied by the XRD, TEM and electron spectroscopy methods, *J. Electron Spectrosc. Relat. Phenom.*, 195, 145–154.
- [18] Iatsenko, A., Sych, O., Nikolenko, A., and Stelmakh, S., 2024, Structure investigation of highly porous bioceramics based on biogenic hydroxyapatite with graphene oxide coating, *Results Surf. Interfaces*, 16, 100265.
- [19] Jiao, X., Qiu, Y., Zhang, L., and Zhang, X., 2017, Comparison of the characteristic properties of reduced graphene oxides synthesized from natural graphites with different graphitization degrees, *RSC Adv.*, 7 (82), 52337–52344.
- [20] Zhang, L., Liang, J., Huang, Y., Ma, Y., Wang, Y., and Chen, Y., 2009, Size-controlled synthesis of graphene oxide sheets on a large scale using chemical exfoliation, *Carbon*, 47 (14), 3365–3368.
- [21] Stankovich, S., Dikin, D.A., Piner, R.D., Kohlhaas, K.A., Kleinhammes, A., Jia, Y., Wu, Y., Nguyen,

- S.B.T., and Ruoff, R.S., 2007, Synthesis of graphene-based nanosheets via chemical reduction of exfoliated graphite oxide, *Carbon*, 45 (7), 1558–6515.
- [22] Khan, S.A., Khan, S.B., Khan, L.U., Farooq, A., Akhtar, K., and Asiri, A.M., 2018, “Fourier Transform Infrared Spectroscopy: Fundamentals and Application in Functional Groups and Nanomaterials Characterization” in *Handbook of Materials Characterization*, Eds. Sharma, S.K., Springer International Publishing, Cham, Switzerland, 317–344.
- [23] Dulyanska, Y., Cruz-Lopes, L., Esteves, B., Guiné, R., and Domingos, I., 2024, FTIR monitoring of polyurethane foams derived from acid-liquefied and base-liquefied polyols, *Polymers*, 16 (15), 2214.
- [24] Kandhol, G., Wadhwa, H., and Verma, A., 2024, Glass transition temperature of agar-reduced graphene oxide (RGO) composites using 2-D contour mapping of temperature dependent FTIR spectra, *Chem. Phys. Impact*, 9, 100690.
- [25] Hosseini, M.A., Malekie, S., and Ebrahimi, N., 2020, The analysis of linear dose-responses in gamma-irradiated graphene oxide: Can FTIR analysis be considered a novel approach to examining the linear dose-responses in carbon nanostructures?, *Radiat. Phys. Chem.*, 176, 109067.
- [26] Sun, H., Yang, Y., and Huang, Q., 2011, Preparation and structural variation of graphite oxide and graphene oxide, *Integr. Ferroelectr.*, 128 (1), 163–170.
- [27] Gurunathan, S., Han, J.W., Park, J.H., Kim, E., Choi, Y.J., Kwon, D.N., and Kim, J.H., 2015, Reduced graphene oxide–silver nanoparticle nanocomposite: A potential anticancer nanotherapy, *Int. J. Nanomed.*, 10 (1), 6257–6276.
- [28] Sherif, H.H.A., El Hotaby, W., Khalil, S.K.H., Hemdan, B.A., and Khalil, W.A., 2023, Preparation, characterization, and biological assessment of functionalized reduced graphene oxide–silver nanocomposite, *J. Mater. Res.*, 38 (7), 1843–1857.
- [29] Viprya, P., Kumar, D., and Kowshik, S., 2023, Study of different properties of graphene oxide (GO) and reduced graphene oxide (rGO), *Eng. Proc.*, 59 (1), 84.
- [30] Lesiak, B., Trykowski, G., Tóth, J., Biniak, S., Kövér, L., Rangam, N., Stobinski, L., and Malolepszy, A., 2020, Chemical and structural properties of reduced graphene oxide—dependence on the reducing agent, *J. Mater. Sci.*, 56 (6), 3738–3754.
- [31] Nongthombam, S., Aruna Devi, N., Sinha, S., Ishwarchand Singh, W., and Swain, B.P., 2023, Analysis of structural defects with the chemical composition of rGO/GaN nanocomposites using Raman spectroscopy, *Mater. Today: Proc.*, 74, 744–749.
- [32] Scardaci, V., and Compagnini, G., 2021, Raman spectroscopy investigation of graphene oxide reduction by laser scribing, *C*, 7 (2), 48.
- [33] Chadha, N., Sharma, R., and Saini, P., 2021, A new insight into the structural modulation of graphene oxide upon chemical reduction probed by Raman spectroscopy and X-ray diffraction, *Carbon Lett.*, 31 (6), 1125–1131.
- [34] Silva Filho, J.C., Venancio, E.C., Silva, S.C., Takiishi, H., Martinez, L.G., and Antunes, R.A., 2020, A thermal method for obtention of 2 to 3 reduced graphene oxide layers from graphene oxide, *SN Appl. Sci.*, 2 (8), 1450.
- [35] Ferrari, A.C., 2007, Raman spectroscopy of graphene and graphite: Disorder, electron–phonon coupling, doping and nonadiabatic effects, *Solid State Commun.*, 143 (1), 47–57.